

LAMOST REVEALS NEPTUNE-SIZE COUSINS OF HOT JUPITERS, PREFERENTIALLY IN
“(METAL-)RICH” AND “ONE-CHILD” *KEPLER* FAMILIES

SUBO DONG,¹ JI-WEI XIE,² JI-LIN ZHOU,² ZHENG ZHENG,³ AND ALI LUO⁴

¹*Kavli Institute for Astronomy and Astrophysics, Peking University, Yi He Yuan Road 5, Hai Dian District, Beijing 100871, China*

²*School of Astronomy and Space Science & Key Laboratory of Modern Astronomy and Astrophysics in Ministry of Education, Nanjing University, 210093, China*

³*Department of Physics and Astronomy, University of Utah, 115 South 1400 East, Salt Lake City, UT 84112, USA*

⁴*National Astronomical Observatories, Chinese Academy of Sciences, Beijing 100012, China*

ABSTRACT

We discover a new population of short-period, Neptune-size planets sharing key similarities with hot Jupiters: both populations are preferentially hosted by metal-rich stars, and both are preferentially found in *Kepler* systems with single transiting planets. We use accurate LAMOST DR4 stellar parameters for main-sequence stars to study the distributions of short-period ($1 \text{ d} < P < 10 \text{ d}$) *Kepler* planets as a function of host star metallicity. The radius distribution of planets around metal-rich stars is more “puffed up” as compared to that around metal-poor hosts. In two period-radius regimes, planets preferentially reside around metal-rich stars, while there are scantily any planets around metal-poor stars. One is the well-known hot Jupiters, and the other is a new population of Neptune-size planets ($2R_{\oplus} \lesssim R_p \lesssim 6R_{\oplus}$), dubbed as “Hoptunes”. Also like hot Jupiters, Hoptunes occur more frequently in systems with single transiting planets than in multiple transiting planetary systems. About 1% of solar-type stars host “Hoptunes”, and the frequencies of Hoptunes and hot Jupiters increase with consistent trends as a function of $[\text{Fe}/\text{H}]$. In the planet radius distribution, hot Jupiters and Hoptunes are separated by a “valley” at approximately Saturn size (in the range of $6R_{\oplus} \lesssim R_p \lesssim 10R_{\oplus}$), and this “hot-Saturn valley” represents an approximately order-of-magnitude decrease in planet frequency compared to hot Jupiters and Hoptunes. The empirical “kinship” between Hoptunes and hot Jupiters suggests likely common processes (migration and/or formation) responsible for their existence.

arXiv:1706.07807v1 [astro-ph.EP] 23 Jun 2017

1. INTRODUCTION

More than two decades after the first surprising discovery (Mayor & Queloz 1995), hot Jupiters still remain to be one of the most hotly studied exoplanet populations. Observationally, they never seem to fail to yield new surprises. It was realized early on that their host stars were predominantly more metal rich than the sun (Gonzalez 1998), and their frequency was later found to strongly correlate with host $[\text{Fe}/\text{H}]$ (Santos et al. 2004; Fischer & Valenti 2005). Lately, *Kepler* data show that they stand out as a distinctly “lonely” population for the dearth of other planets on nearby orbits in their systems (Steffen et al. 2012; Huang et al. 2016). Despite the plethora of observational findings, we still do not know their origins with certainty – we do not know how they migrate to their present close-in orbits ($P \lesssim 10$ d) (see review by Winn & Fabrycky 2015) or if they have migrated at all (Batygin et al. 2016; Boley et al. 2016).

More clues about their origins may come from examining them in the context of planet distributions and the dependence of such distributions on host environment: How unique are the conditions forming hot Jupiters? And do hot Jupiters have “relatives”, which share similarities in their planetary and host-star properties?

With thousands of planets discovered from monitoring $\sim 200,000$ target stars, the *Kepler* mission has unprecedented potential to study planet distributions over a wide range of parameter space and their possible links to stellar properties (see e.g., Howard et al. 2012; Dong & Zhu 2013; Fressin et al. 2013; Petigura et al. 2013; Burke et al. 2015; Wang & Fischer 2015; Zhu et al. 2016). However, making any reliable statistical inference with a large *Kepler* sample is seriously limited by the lack of accurate stellar parameters for the majority of the targets. For most of the *Kepler* targets, stellar parameters are only available via the Kepler Input Catalog (KIC; Brown et al. 2011), whose $[\text{Fe}/\text{H}]$ and $\log g$ measurements are known to have large uncertainties and serious systematic errors (see, e.g. Dong et al. 2014; Plavchan et al. 2014; Xie et al. 2016; Petigura et al. 2017). Significant efforts have been put into characterizing planet hosts by taking high-resolution spectroscopy (e.g., Buchhave et al. 2012; Petigura et al. 2017) or extracting asteroseismic parameters (e.g., Huber et al. 2013). But the accurate parameters of the underlying parent sample (with and without detected planets) are poorly known, which presents a major uncertainty in *Kepler* planet statistics (see relevant discussions in Dong & Zhu 2013; Burke et al. 2015) and also makes it difficult to reliably derive planet distributions as a function of stellar parameters.

With 4000 fibers and 5° diameter field of view, the 4m Large Sky Area Multi-Object Fiber Spectroscopic Tele-

scope (LAMOST, a.k.a. Goushoujing Telescope) (Wang et al. 1996; Su & Cui 2004; Cui et al. 2012; Zhao et al. 2012) is uniquely positioned to perform a systematic spectroscopic survey of *Kepler* target stars. The “LAMOST-*Kepler* project” (De Cat et al. 2015; Ren et al. 2016) attempts to observe all *Kepler* target stars with no preference for known planet hosts. It forms a large and unbiased sample to perform statistical inference on planet distributions and correlations with host properties (Dong et al. 2014). For main-sequence stars, the stellar parameters inferred from the official LASP pipeline (Luo et al. 2015) are demonstrated to be accurate (typical uncertainties: $\sigma T_{\text{eff}} = 100\text{K}$, $\sigma \log g = 0.1-0.15$ dex, $\sigma[\text{Fe}/\text{H}] = 0.1$ dex) from comparisons with high-resolution spectroscopic and asteroseismic parameters (see Section 1 of Supporting Information of Xie et al. 2016 and also Dong et al. 2014; Wang et al. 2016.) The accurate LASP stellar parameters make possible the study of the metallicity distribution of *Kepler* targets (Dong et al. 2014) and the eccentricity distribution of *Kepler* planets (Xie et al. 2016). Wang et al. (2017) use LASP parameters to study host metallicity for Earth-size planets. Stellar parameters have also been extracted from LAMOST spectra using pipelines other than the official LASP, such as LSP3 (Xiang et al. 2015) and ROTFIT (Frasca et al. 2016). Using ROTFIT parameters, Mulders et al. (2016) found that on average the hosts for hot Earth-size planets have super-solar metallicity.

We study host metallicity distribution for *Kepler* planets in the period range of $1\text{ d} < P < 10\text{ d}$ using the LAMOST/LASP stellar parameters (Luo et al. 2015) from Data Release 4 (DR4), which contains data for $\sim 60,000$ AFGK-type *Kepler* stars ($\sim 30\%$ of all *Kepler* targets). Previous studies (Beaugé & Nesvorný 2013; Mazeh et al. 2016) have identified a “desert” of short-period ($2-4$ d and it may extend to $5-10$ d) Neptunes by studying samples from Radial-Velocity (RV) surveys, mixed ground-based and *Kepler* transit searches. We benefit from the homogeneity of the *Kepler* sample with well quantified detection efficiencies as well as accurate stellar and planetary parameters thanks to LAMOST, and this work is focused on the effects of metallicity.

We discover a “cousin” population of hot Jupiters: like hot Jupiters, these short-period Neptune-size planets ($2R_{\oplus} \lesssim R_p \lesssim 6R_{\oplus}$), dubbed as “Hoptunes”, are predominantly hosted by metal-rich stars, and they also reside more often in single transiting than multiple transiting planetary systems. In the radius distribution the populations of hot Jupiters and Hoptunes frame a “valley” at approximately Saturn size (in the range of $6R_{\oplus} \lesssim R_p \lesssim 10R_{\oplus}$), and in this “hot-Saturn valley” there is a significant deficit in planet frequency.

2. SAMPLE SELECTION

We select our stellar sample using the official LASP (Luo et al. 2015) parameters from LAMOST DR4 AFGK stellar catalog. The stars satisfy $4700K < T_{\text{eff}} < 6500K$ and $\log g > 4.0$ so that our sample consists primarily of solar-type main-sequence stars. They also cover a range of stellar parameters for which we have comparison stars available with accurate high-resolution spectroscopic parameters (Dong et al. 2014; Xie et al. 2016). Our stellar sample consists of 30,727 stars in total. Stellar masses and radii are derived by isochrone fitting as described in Xie et al. (2016). We then cross-match with the catalog of *Kepler* planet candidates and remove the known false positives and those with large false positive probabilities (FPPs). Stellar parameters derived from LAMOST/LASP are applied to derive the planet properties such as planet radius R_p , which has a typical error of about 15%. We focus on those with orbital period $1\text{d} < P < 10\text{d}$ and planet radius $1R_{\oplus} < R_p < 20R_{\oplus}$. The sample has 295 planets in 256 systems. 151 planets are in systems that contain single *Kepler* transiting planets, and 144 planets are in multiple transiting planet systems where the other transiting planets in the systems are not necessarily in the above-mentioned period and radius ranges. In the Appendix, we provide more details on sample selection, and we also show that the main results discussed below are not sensitive to the exact choices of sample selection.

3. ANALYSIS & RESULTS

We divide the stellar sample into two metallicity subsamples: metal rich ($[\text{Fe}/\text{H}] \geq 0$) and metal poor ($[\text{Fe}/\text{H}] < 0$). Figure 1 shows the distributions of period and planet radius for the planets that belong to the two subsamples, respectively.

In the metal-poor subsample, except for a handful of objects, almost all the planets lie in the bottom part of the period-radius plane: for those with $1\text{d} < P < 3\text{d}$, their radii are smaller than about $\approx 2R_{\oplus}$, and for those with $3\text{d} < P < 10\text{d}$, the upper boundary in radius grows from $\approx 2R_{\oplus}$ to $\approx 4R_{\oplus}$ with increasing period. This boundary is approximately illustrated as a broken magenta line connecting $(P, R_p) = (1, 2)$ with $(3, 2)$ with $(10, 4)$ on the period-radius plane. At $P > 3\text{d}$, this boundary is similar to the lower boundary of the “desert” described in Mazeh et al. (2016) (see Figure 8 in the Appendix). In the metal-rich subsample, about 3/4 of the planets are concentrated below the broken magenta line. The rest $\sim 1/4$ of all planets in the metal-rich subsample reside in the parameter space that is scantily populated with planets for the metal-poor subsample. One population of planets hosted by these metal-rich

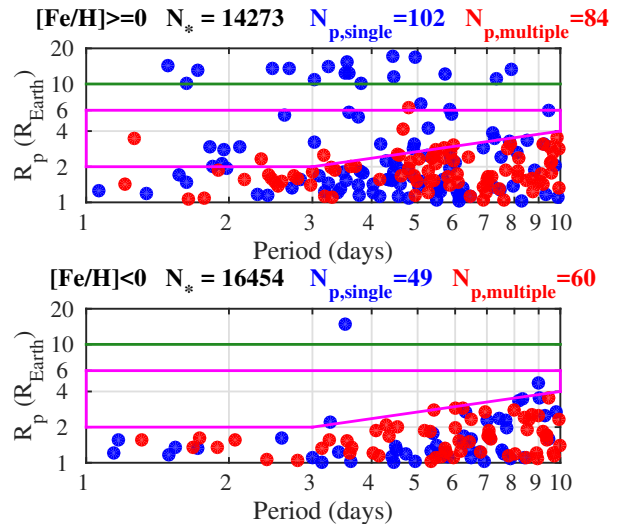


Figure 1. Period-radius distribution for short-period *Kepler* planet candidates hosted by metal-rich (top) and metal-poor (bottom) stars. Planets in single and multiple transiting planetary systems are plotted in blue and red circles, respectively. The numbers of planets and stars (including non-transiting targets) are printed on the top of each panel. The green horizontal line ($R_p = 10R_{\oplus}$) denotes the empirical lower boundary of hot Jupiter, and the magenta lines denote the empirical boundaries of Hoptunes (see Section 3). Note that the typical uncertainty in R_p is about 15%.

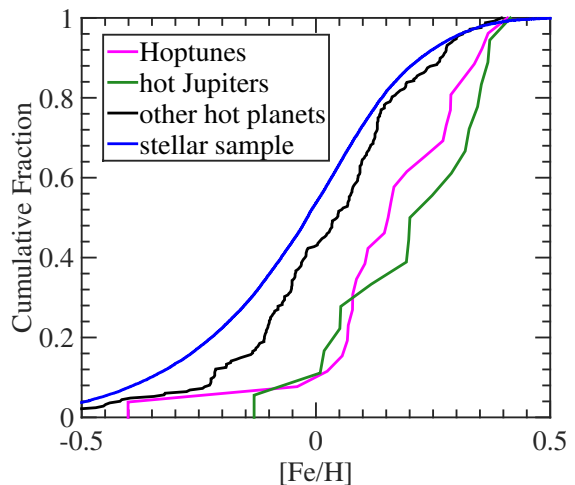


Figure 2. Cumulative fractions as a function of host $[\text{Fe}/\text{H}]$. Hoptunes (magenta) and hot Jupiters (green) have similar distributions, and using the two-sample K-S test, the two samples are drawn from the same underlying distribution with a probability of 45%. In contrast, the distributions for both Hoptunes and hot Jupiters are different from those of the stellar sample (blue) and other planets (black) at high statistical significances.

stars have radii larger than $\sim 10R_{\oplus}$ (marked by a green

solid line), and they are the hot Jupiters. The other population hosted by metal-rich stars have radii smaller than $\sim 6 R_{\oplus}$ while larger than those indicated by the bottom broken magenta line. Their sizes ($2 - 6 R_{\oplus}$) are close to that of the Neptune at about $4 R_{\oplus}$, but we do not know whether all of them are physically Neptune-like planets. Given the uncertainties in their physical states (Neptunes, Super-Earths, mini-Neptunes, or other possibilities), we choose to dub this population as “Hoptunes” in the text.

Next we discuss three main features in the distributions, including two striking similarities between Hoptunes and hot Jupiters, and a significant “valley” separating them in the radius distribution.

1) Hoptunes and hot Jupiters are both preferentially hosted by metal-rich stars, and for both populations the planet frequencies correlate with the host [Fe/H].

The contrast between metal-rich and metal-poor stars in hosting hot Jupiters and Hoptunes is statistically significant. In the metal-rich subsample, there are 17 hot Jupiters and 24 Hoptunes, which are $9.1^{+2.8}_{-2.2}\%$ and $12.9^{+3.2}_{-2.6}\%$ of all planets in that subsample, respectively. If the metal-poor subsample had similar relative fractions of these two populations, we would expect to see $10.0^{+3.0}_{-2.4}$ hot Jupiters and $14.1^{+3.5}_{-2.9}$ Hoptunes, but there are only 1 hot Jupiter and 2 Hoptunes detected. Figure 2 shows the cumulative fraction of various planet hosts and the stellar sample as a function of [Fe/H]. The strong dependence of hot Jupiters’ occurrence on host-star metallicity is well known, and such a dependence is clearly seen from our sample. As compared with the stellar sample as well as “other hot planets” (i.e., not hot Jupiters or Hoptunes), the hot Jupiters are preferentially hosted by metal-rich stars. Using the two-sample Kolmogorov-Smirnov (K-S) tests, the [Fe/H] distributions of hot Jupiters are inconsistent with drawing from the same sample for the stellar sample and “other hot planets” (at p-values of 0.003% and 0.032%, respectively). Hoptunes have similarly strong preference for metal-rich hosts, and their distributions are inconsistent with the stellar sample and “other hot planets” with even higher statistical significance (at p-values of 0.0004% and 0.026%, respectively). Hot Jupiters and Hoptunes are consistent with being drawn from the same sample using the two-sample K-S test, resulting a p-value of 45%. The distribution of “other hot planets”, dominated by Earth-size planets ($1R_{\oplus} < R_p < 2R_{\oplus}$), is also more skewed (though in a degree significantly less than hot Jupiters and Hoptunes) toward higher metallicities as compared to the stellar sample (the K-S test p-value = 0.2%), which is qualitatively consistent with

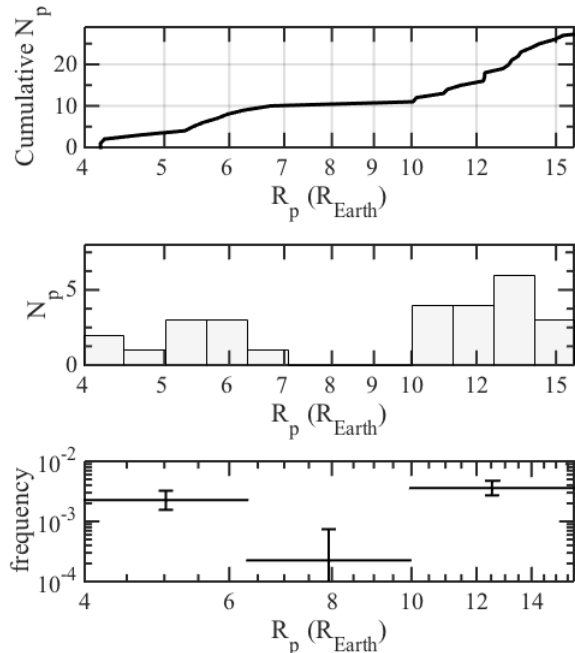


Figure 3. The hot-Saturn valley revealed from the radius distribution of planets in our sample. Top: Cumulative distribution of planets with radii larger than $4 R_{\oplus}$. Middle: Number of detected planets in radius bins with equal size in logarithm. Bottom: Intrinsic planet frequencies as a function of planetary radius.

the conclusion by Mulders et al. (2016) that there is a preference of metal-rich hosts for hot Earths. Later in this section we derive the intrinsic frequencies by taking into account the incompleteness of *Kepler*.

2) Hoptunes and hot Jupiters both tend to preferentially exist in *Kepler*’s single transiting planetary systems.

A distinguishing feature of hot Jupiters is that they tend not to have neighboring planets in close-by orbits (Steffen et al. 2012; Huang et al. 2016). All the hot Jupiters in our sample are single transiting planet systems, and the majority of the Hoptunes are in *Kepler* singles ($73 \pm 9\%$ with the uncertainty estimated from binomial distribution). In contrast, in the regimes under the broken magenta lines, slightly less than half of planets ($45 \pm 3\%$) are in single transiting planetary systems – note that the single fraction are similar for **both** metal-poor and metal-rich subsamples, approximately $46 \pm 4\%$ for metal-poor and $43 \pm 5\%$ for metal-rich. Therefore, like hot Jupiters, Hoptunes are also preferentially in singles compared to other hot planets. Using a likelihood analysis based on binomial distribution, we also find that the single fraction of Hoptunes is statisti-

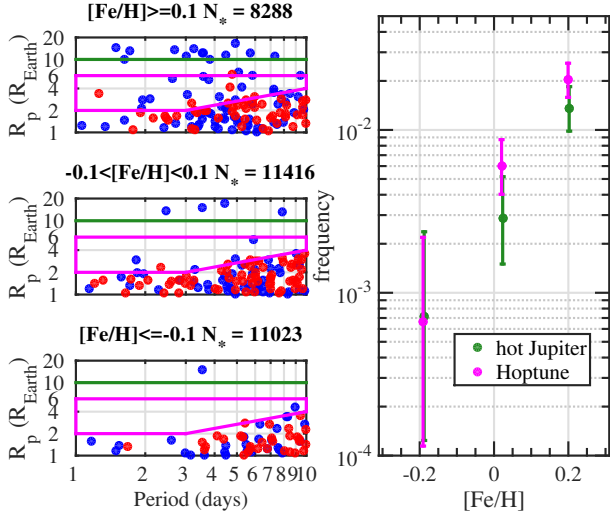


Figure 4. The dependence of planet distribution (Left Panel) and intrinsic frequency (Right Panel) on stellar metallicity ($[\text{Fe}/\text{H}]$) using three metallicity subsamples. The frequencies of hot Jupiters and Hoptunes have similar trends as a function of metallicity – for both populations, they increase by a factor ~ 10 from the “sub-solar” metallicity regime ($[\text{Fe}/\text{H}] \leq -0.1$) to the super-solar ($[\text{Fe}/\text{H}] \geq 0.1$) regime, and the frequencies of Hoptune are similar (within a factor of ~ 2) to those of hot Jupiters for all subsamples.

cally significantly smaller than that of hot Jupiters, at a 2.9σ significance.

3) Hoptunes and hot Jupiters are separated by a “hot-Saturn valley”.

As can be seen in Figure 1, there is a deficit of planets near Saturn size (about $6\text{--}10 R_{\oplus}$) in the planet-radius distributions between the Hoptunes and hot Jupiters, and we refer this deficit as the “hot-Saturn valley”. The hot-Saturn valley can be clearly seen in the cumulative distribution of planet radius for planets with $R_p > 4 R_{\oplus}$ from our sample (upper panel of Figure 3). The cumulative distribution has two clear breaks occurring at $\sim 6.5 R_{\oplus}$ and $\sim 10 R_{\oplus}$, and between these breaks, planets occur significantly less frequently compared to other ranges of radii. In the middle panel of Figure 3, we show a histogram of observed radius distribution with 12 uniformly spaced bins in logarithm. The four bins closest to $8 R_{\oplus}$ have 1 planets where the four bins on the left (Hoptunes) have 10 planets and the four bins on the right (hot Jupiters) have 16 planets. This deficit of planets near Saturn size is unlikely due to random fluctuations – assuming that the bins around Saturn size have equal occurrence of planets as in the left and right bins, the Poisson probabilities are 0.05% and 0.0002%, respectively.

Finally we consider the incompleteness of *Kepler* survey and calculate the intrinsic planet frequency for our sample. We take the survey selection, which is the incompleteness due to the survey detection thresholds, and the transit geometric bias into account. In order to calculate the incompleteness, we use the code supplied by Burke et al. (2015) based on the detection efficiency characterization method of Christiansen et al. (2015), and we apply the LAMOST stellar parameters in the calculations.

To better examine the dependence of the planet frequency on metallicity, we divide the sample according to $[\text{Fe}/\text{H}]$ into three subsamples – “super solar” ($[\text{Fe}/\text{H}] \geq 0.1$), “solar” ($-0.1 < [\text{Fe}/\text{H}] < 0.1$) and “sub solar” ($[\text{Fe}/\text{H}] \leq -0.1$). The planet period-radius distributions for three metallicity subsamples are shown in the left three panels of Figure 4. In the “sub-solar” subsample (the bottom-left panel), there are only a handful of hot Jupiters and Hoptunes. Then in the “solar” subsample (the middle-left panel), there are several hot Jupiters, and a few Hoptunes start to emerge close to the lower boundary (the broken magenta line). Finally, in the “super-solar” subsample (the upper-left panel), there is a dramatic increase in the numbers for both hot Jupiters and Hoptunes. The right panel shows the intrinsic frequencies of hot Jupiters and Hoptunes after correcting the survey incompleteness and geometric biases. The frequencies of Hoptunes and hot Jupiters increase dramatically (by a factor of ~ 10 from “sub-solar” to “super-solar”) with $[\text{Fe}/\text{H}]$. Such a trend for hot Jupiter hosts is well known (see e.g. Guo et al. 2017 and the references therein), and the trend for Hoptune hosts is remarkably similar. The frequencies of Hoptunes are similar (within a factor of ~ 2) to that of hot Jupiters for all subsample. Hosts of Hoptunes and hot Jupiters have similarly strong preferences for host metallicities higher than the sun (“super-solar” vs. “solar”).

The bottom panel of Figure 3 shows the intrinsic frequencies of planets within the $\log(R_p)$ bins spanning 0.2 dex around $\sim 5 R_{\oplus}$, $\sim 8 R_{\oplus}$ and $\sim 12 R_{\oplus}$ in our sample. The averaged frequencies of the planets in these subsamples are $0.23^{+0.10}_{-0.07}\%$, $0.02^{+0.05}_{-0.02}\%$, $0.36^{+0.10}_{-0.09}\%$ at approximately Neptune size, Saturn size and Jupiter size, respectively. Thus the hot-Saturn valley represents an approximately one order of magnitude depression in planet frequency as a function of planet radius. The averaged planet frequencies $dN_p/d\log(R_p)d\log(P)$ for hot Jupiters and Hoptunes in these subsamples are consistent within the uncertainties.

4. DISCUSSION

Our findings benefit from the homogeneity of the *Kepler* sample as well as accurate planet radii and host metallicities thanks to the high accuracy of LAMOST stellar parameters. Beugé & Nesvorný (2013) and Mazeh et al. (2016) found a desert of short-period Neptunian planets using mixed samples of planets discovered from various surveys. The upper boundary of the desert defined by Mazeh et al. (2016) is similar to that of the hot-Saturn valley we identify in this work (see Figure 8 in the Appendix). While this upper boundary from Mazeh et al. (2016) is a slant line on the period-radius plane based on a large number of planets mostly contributed from ground-based transits, our sample is too small to clearly determine a slope. Their lower boundary resembles with the lower boundary of Hoptunes, especially for $P > 3$ d. According to our results, their desert appears to encompass both the hot-Saturn valley and the Hoptunes. Inside their desert, we find that Hoptunes have a similar averaged frequency of $\sim 1\%$ as hot Jupiters. In comparison, hot-Saturn valley has an order-of-magnitude deficit in planet frequency. These features appear to be largely “washed out” in mixed transiting-planet samples used by Mazeh et al. (2016).

The similarities in host metallicity, intrinsic frequency and preference for single transiting planetary systems suggest an likely close link between hot Jupiters and Hoptunes in their migration and/or formation processes.

The correlation between the intrinsic frequency of short-period Jupiter and stellar metallicity has been well established (Santos et al. 2004; Fischer & Valenti 2005). According to core-accretion models, the total masses of building-block planetesimals and/or embryos are proportional to those of the heavy elements in the host stars (Ida & Lin 2004). One possible interpretation of the metallicity correlation for short-period Jupiters is that, the metal-rich environment provides more building blocks to form massive planetary cores ($\sim 10 M_{\oplus}$) before the gas disk dissipates, which are crucial for gas accretion to form giant planets like hot Jupiters (Pollack et al. 1996). However, such an interpretation may not be well suitable for the metallicity correlation of Hoptunes, since for most Hoptunes, especially those smaller ones with radius less than $4R_{\oplus}$, they do not need massive cores to accrete as much gas as needed for forming Jupiters. Another possibility is that metallicity may play an important role to trigger/amplify certain migration mechanisms for hot Jupiters (Dawson & Murray-Clay 2013; Liu et al. 2016). Such mechanisms should then similarly operate for Hoptunes and also preferentially produce single transiting planetary systems. Note that we find at 2.9σ significance that the fraction of single-transiting planet systems of hot Jupiters is higher

than that of Hoptunes, indicating that whatever process removes the “brothers” of hot Jupiters likely operate less efficiently for Hoptunes. The in-situ formation mechanisms (e.g., Hansen & Murray 2012) are also subject to these constraints too.

The hot-Saturn valley identified in this work broadly agrees with the bimodal planetary radius distribution expected from planet population synthesis simulations (e.g., Mordasini et al. 2012). The radius range of the hot-Saturn valley ($R_p \sim 6-10R_{\oplus}$) roughly corresponds to the mass domain (between $\sim 10-30$ and $\sim 100-200 M_{\oplus}$) of the “planet desert” at less than ~ 3 AU expected from core accretion simulations of planet formation (Ida & Lin 2004; Mordasini et al. 2009).

When studying the radius distribution for short-period planets, it is important to consider the effects of planetary inflation (e.g., Lopez & Fortney 2016 and the references therein) and/or evaporations (Baraffe et al. 2005; Owen & Wu 2013; Jin et al. 2014). Baraffe et al. (2005) suggest that hot Neptunes may originate from evaporation of hot Jupiters, and thus they may share common origins and evolution history. This hypothesis is consistent with the similarities between hot Jupiters and Hoptunes found in this work. In addition, it may be interesting to test whether mechanisms such as photo-evaporation can be responsible in shaping features such as the sharp lower boundary for Hoptunes (the broken magenta line in Figure 1) in the period-radius distribution and also explain how the sharpness of this boundary varies with host metallicity. For instance, the consequence of photo-evaporation may depend on planet core mass (Owen & Wu 2013; Jin et al. 2014), and one may speculate that core mass distribution can differ according to host $[\text{Fe}/\text{H}]$ thus can potentially play a role in forming the $[\text{Fe}/\text{H}]$ -dependent planet distribution found here. RV follow-ups of Hoptunes can provide the crucial mass measurements to reveal their physical states and test such scenarios.

The “kinship” between hot Jupiters and Hoptunes as well as the hot-Saturn valley separating these two cousins offer new clues and constraints for the formation and migration of short-period planets. Future surveys and missions, particularly TESS, are expected to detect many more short-period planets and explore these features with greater details.

We thank A. Gould for stimulating discussions and insights into statistics. We are grateful to B. Katz, K. Stanek, S. Kozłowski, C. Mordasini and D. Lin for helpful comments. S.D. acknowledges Project 11573003 supported by NSFC and the LAMOST Fellowship, which is supported by Special Funding for Advanced Users,

budgeted and administrated by Center for Astronomical Mega-Science, Chinese Academy of Sciences (CAS). J.-W.X. and J.-L.Z. acknowledge support from the Key Development Program of Basic Research of China (973 Program, Grant 2013CB834900) and the NSFC Grants 11333002. J.-W.X. is also supported by the NSFC Grant 11403012 and a Foundation for the Author of National Excellent Doctoral Dissertation of People’s Republic of

China. Guoshoujing Telescope (the Large Sky Area Multi-Object Fiber Spectroscopic Telescope; LAMOST) is a National Major Scientific Project built by the CAS. Funding for the project has been provided by the National Development and Reform Commission. LAMOST is operated and managed by the National Astronomical Observatories, CAS.

APPENDIX

A. SAMPLE SELECTION

We cross-match between the AFGK Stars Catalog of LAMOST DR4 and all target stars observed during Q1-Q16 of the *Kepler* mission. As a result, there are 59,964 unique *Kepler* target stars with LAMOST LASP stellar parameters. We pick stars satisfying $4700K < T_{\text{eff}} < 6500K$ and $\log g > 4.0$ so that the stellar sample is mostly main-sequence stars, and 30,727 stars survive the cut (green points the A1 panel of Figure 5). We also test other selection criteria of the stellar samples to check if they affect our main results. In one test, we choose $\log g > 4.3$ to more aggressively remove sub giants in the sample (green points the A2 panel of Figure 5). In another test, we use a sloped upper boundary in $T_{\text{eff}}\text{-}\log g$ (green points in the A3 panel). The resulting planet distributions for $[\text{Fe}/\text{H}] \geq 0$ and $[\text{Fe}/\text{H}] < 0$ are plotted in B2) and C2), B3) and C3) panels, respectively. The main results of the paper remain the same and are not sensitive to the specific choice of the stellar sample.

We cross-match the LAMOST AFGK catalog with the Kepler planet-candidate catalog. We primarily use the planet sample from Q1-Q16 (Mullally et al. 2015), which has well quantified detection efficiencies (Christiansen et al. 2015; Burke et al. 2015). The following updated catalog DR 24 (Coughlin et al. 2016) is flawed for occurrence rate calculations (Christiansen et al. 2016). The most recent catalog DR 25 (Twicken et al. 2016) is not yet finalized at the time of our work. There are 2422 Kepler Object of Interests (KOIs) in 1996 systems with LAMOST stellar parameters. Then we apply a series of selections. First of all, we attempt to remove false positives (FPs). We remove KOIs if they are identified as FPs according any of the following references: the Q1-Q16 catalog (Mullally et al. 2015), the DR 24 catalog (Coughlin et al. 2016), the DR 25 catalogs (Twicken et al. 2016), and the SOPHIE RV follow-up survey of giant planets (Santerne et al. 2016). For the planet sample analyzed in the main text, we also follow Xie et al. (2016) and remove the candidates with large False Positive Probabilities $\text{FPP} > 68\%$ in the Kepler Astrophysical False Positive Probabilities Table (Morton et al. 2016). We note that eliminating candidates with too small FPP may potentially bias planet statistics by significantly removing a large fraction of true planets (e.g., $\text{FPP} = 10\%$ means that 90% probability being true planets). Nevertheless, we also test removal of candidates with $\text{FPP} > 1\%$ while keeping all other criteria unchanged. As shown in Figure 6, the resulting distribution (right two panels) hardly differ from that of the default planet sample (left two panels). We also remove KOIs with transit signal-to-noise ratios (SNRs) smaller than 7.1 and radius $R_p > 20R_{\oplus}$. After these cuts, we are left with 1218 KOIs in 913 systems. Next, we apply the same stellar parameter cut as the stellar sample ($4700K < T_{\text{eff}} < 6500K$ and $\log g > 4.0$), and then we have 945 KOIs in 686 systems. Finally, we only analyze planets with periods between 1 and 10 days and radii greater than $1 R_{\oplus}$. The reason for excluding planets with periods shorter than 1 d is because the standard Kepler pipeline is not well conditioned to detect these ultra short period (USP) KOIs (Jackson et al. 2013; Sanchis-Ojeda et al. 2014; Adams et al. 2016). Finally, we obtain a sample with 295 planets in 256 systems.

As discussed in the main text, accurate LAMOST stellar parameters are the key to carry out this study. Figure 7 shows the distributions of the planet candidates in our sample when KIC stellar parameters are used. Due to the large uncertainties and systematic errors in $\log g$ and $[\text{Fe}/\text{H}]$, it is impossible to identify the patterns in planet distributions discovered in this work.

The planet detection efficiency is calculated using the Python code (<https://github.com/christopherburke/KeplerPORTs>) by Burke et al. (2015) with stellar parameters replaced by those of the LAMOST. R_* and M_* are derived following the methods described in Xie et al. (2016). It is worth noting that the survey efficiencies are essentially the same in the regimes of interests for metal-rich and metal-poor systems (Figure 8).

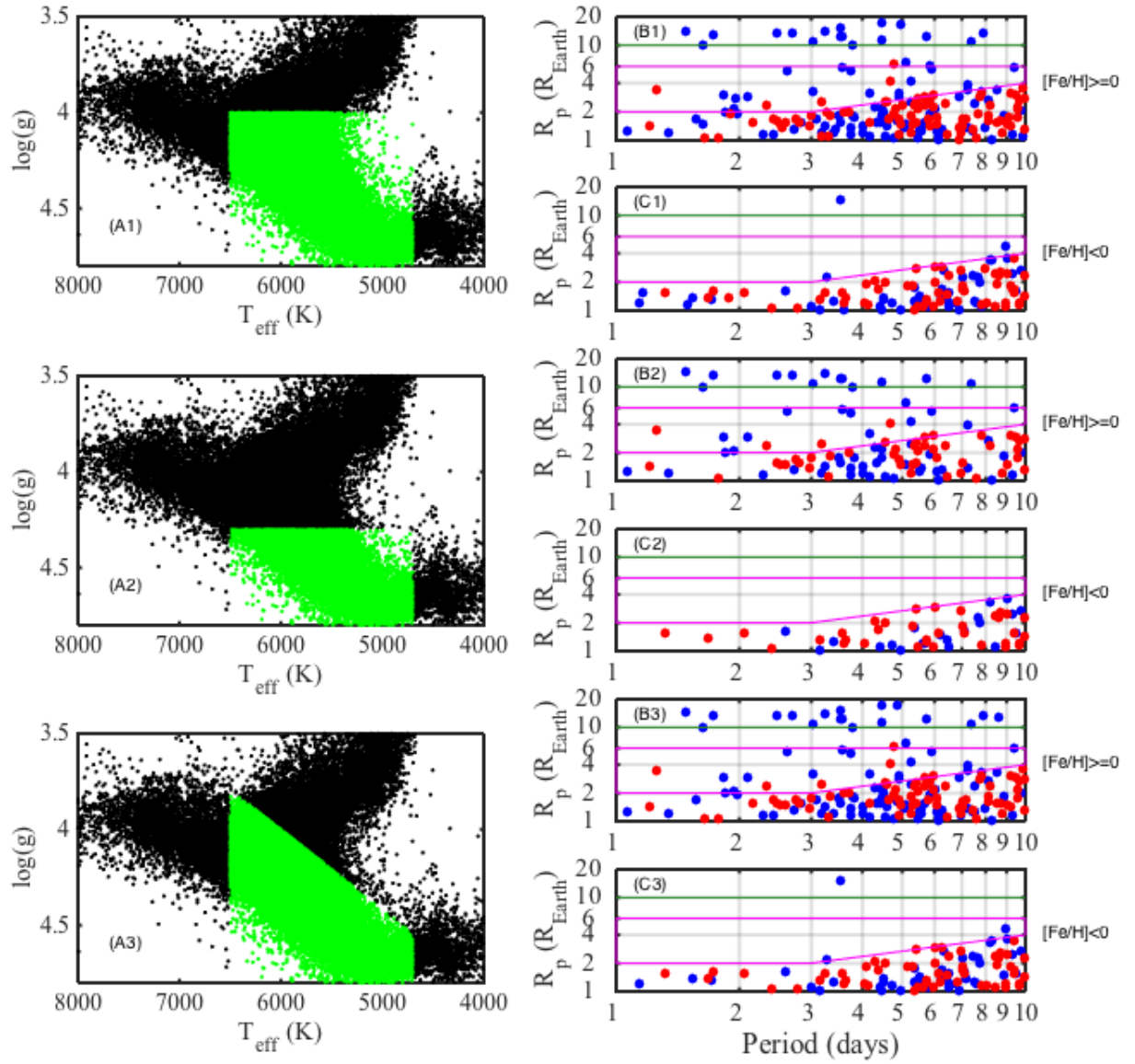


Figure 5. Stellar sample selections and tests. The green dots in Panel (A1) show the star selected in the main text, and they satisfy $4700K < T_{\text{eff}} < 6500K$ and $\log g > 4.0$. We test the effects of alternative selections. The green dots in Panel (A2) show a more stringent criterion of $\log g > 4.3$ to more aggressively remove sub giants. The resulting distributions in planets (B2 and C2) are similar to those from the default sample shown in panels B1 and C1. The results (shown in B3 and C3) are similar for sloped upper boundary in T_{eff} and $\log g$ plane (A3).

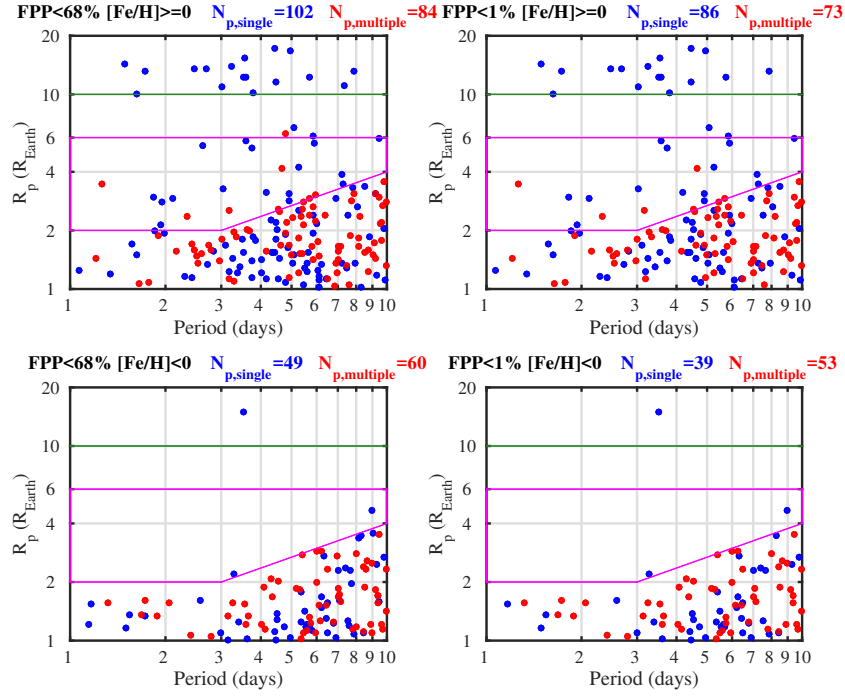


Figure 6. The right panels show the resulting planet distributions for a more stringent cut for False Positive Probability $\text{FPP} < 1\%$, and the result distributions are similar in main features with the default selection criteria $\text{FPP} < 68\%$.

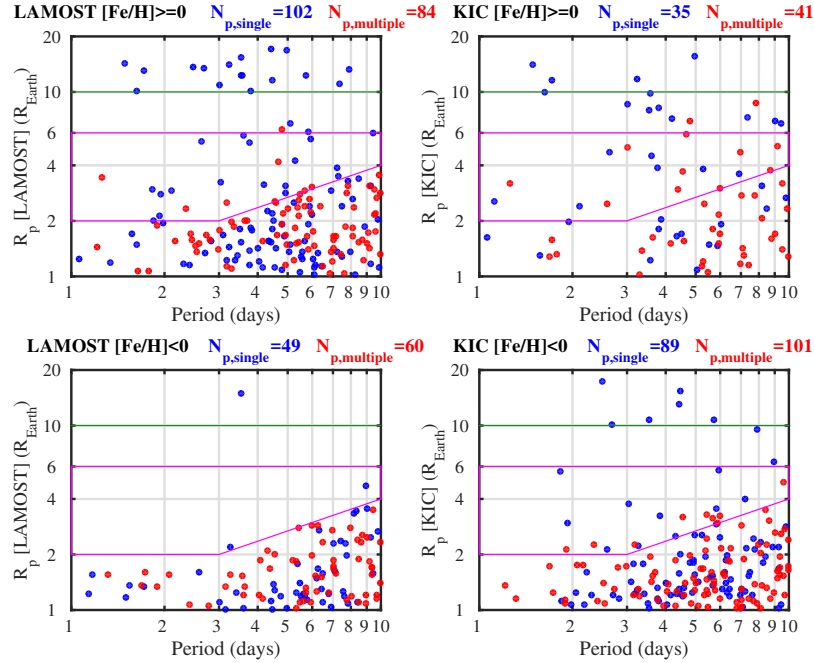


Figure 7. The right panels show the planet distributions when the stellar parameters from the KIC catalog are adopted. Due to the large uncertainties and systematics in the KIC parameters, it is impossible to identify the main patterns in the planet distributions concluded in this work using the accurate LAMOST parameters (the left panels).

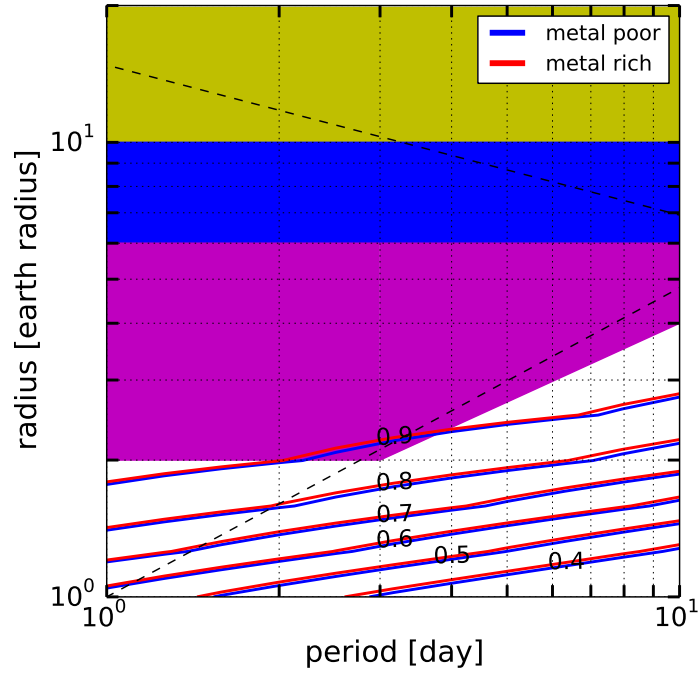


Figure 8. The Kepler survey efficiency for the metal poor ($[\text{Fe}/\text{H}] < 0$) and metal rich ($[\text{Fe}/\text{H}] \geq 0$) subsamples are shown as contours in blue and red, respectively, in the period-radius diagram. The efficiencies are nearly identical for the two subsamples in the regimes of our interest. The regimes of Hoptunes, hot Saturns and hot Jupiters are filled in purple, blue and green, respectively. The detection efficiencies in these three regions are close to 100%. We also plot the boundaries of the “desert” identified by [Mazeh et al. \(2016\)](#) with black dashed lines.

REFERENCES

- Adams, E. R., Jackson, B., & Endl, M. 2016, *AJ*, 152, 47
- Baraffe, I., Chabrier, G., Barman, T. S., et al. 2005, *A&A*, 436, L47
- Batygin, K., Bodenheimer, P. H., & Laughlin, G. P. 2016, *ApJ*, 829, 114
- Beaugé, C., & Nesvorný, D. 2013, *ApJ*, 763, 12
- Boley, A. C., Granados Contreras, A. P., & Gladman, B. 2016, *ApJL*, 817, L17
- Brown, T. M., Latham, D. W., Everett, M. E., & Esquerdo, G. A. 2011, *AJ*, 142, 112
- Buchhave, L. A., Latham, D. W., Johansen, A., et al. 2012, *Nature*, 486, 375
- Burke, C. J., Christiansen, J. L., Mullally, F., et al. 2015, *ApJ*, 809, 8
- Chabrier, G., Baraffe, I., Leconte, J., Gallardo, J., & Barman, T. 2009, 15th Cambridge Workshop on Cool Stars, Stellar Systems, and the Sun, 1094, 102
- Christiansen, J. L., Clarke, B. D., Burke, C. J., et al. 2015, *ApJ*, 810, 95
- Christiansen, J. L., Clarke, B. D., Burke, C. J., et al. 2016, *ApJ*, 828, 99
- Coughlin, J. L., Mullally, F., Thompson, S. E., et al. 2016, *ApJS*, 224, 12
- Cui, X.-Q., Zhao, Y.-H., Chu, Y.-Q., et al. 2012, *Research in Astronomy and Astrophysics*, 12, 1197
- Dawson, R. I., & Murray-Clay, R. A. 2013, *ApJL*, 767, L24
- Dong, S., & Zhu, Z. 2013, *ApJ*, 778, 53
- Dong, S., Zheng, Z., Zhu, Z., et al. 2014, *ApJL*, 789, L3
- De Cat, P., Fu, J. N., Ren, A. B., et al. 2015, *ApJS*, 220, 19
- Fischer, D. A., & Valenti, J. 2005, *ApJ*, 622, 1102
- Frasca, A., Molenda-Żakowicz, J., De Cat, P., et al. 2016, *A&A*, 594, A39
- Fressin, F., Torres, G., Charbonneau, D., et al. 2013, *ApJ*, 766, 81
- Gonzalez, G. 1998, *A&A*, 334, 221
- Guo, X., Johnson, J. A., Mann, A. W., et al. 2017, *ApJ*, 838, 25
- Hansen, B. M. S., & Murray, N. 2012, *ApJ*, 751, 158
- Howard, A. W., Marcy, G. W., Bryson, S. T., et al. 2012, *ApJS*, 201, 15
- Huang, C., Wu, Y., & Triaud, A. H. M. J. 2016, *ApJ*, 825, 98
- Huber, D., Chaplin, W. J., Christensen-Dalsgaard, J., et al. 2013, *ApJ*, 767, 127
- Ida, S., & Lin, D. N. C. 2004, *ApJ*, 604, 388
- Ida, S., & Lin, D. N. C. 2004, *ApJ*, 616, 567
- Jackson, B., Stark, C. C., Adams, E. R., Chambers, J., & Deming, D. 2013, *ApJ*, 779, 165
- Jin, S., Mordasini, C., Parmentier, V., et al. 2014, *ApJ*, 795, 65
- Liu, B., Zhang, X., & Lin, D. N. C. 2016, *ApJ*, 823, 162
- Lopez, E. D., & Fortney, J. J. 2016, *ApJ*, 818, 4
- Luo, A.-L., Zhao, Y.-H., Zhao, G., et al. 2015, *Research in Astronomy and Astrophysics*, 15, 1095
- Mayor, M., & Queloz, D. 1995, *Nature*, 378, 355
- Mayor, M., Marmier, M., Lovis, C., et al. 2011, *arXiv:1109.2497*
- Mazeh, T., Holczer, T., & Faigler, S. 2016, *A&A*, 589, A75
- Mordasini, C., Alibert, Y., & Benz, W. 2009, *A&A*, 501, 1139
- Mordasini, C., Alibert, Y., Georgy, C., et al. 2012, *A&A*, 547, A112
- Morton, T. D., Bryson, S. T., Coughlin, J. L., et al. 2016, *ApJ*, 822, 86
- Mulders, G. D., Pascucci, I., Apai, D., Frasca, A., & Molenda-Żakowicz, J. 2016, *AJ*, 152, 187
- Mullally, F., Coughlin, J. L., Thompson, S. E., et al. 2015, *ApJS*, 217, 31
- Owen, J. E., & Wu, Y. 2013, *ApJ*, 775, 105
- Petigura, E. A., Howard, A. W., & Marcy, G. W. 2013, *Proceedings of the National Academy of Science*, 110, 19273
- Petigura, E. A., Howard, A. W., Marcy, G. W., et al. 2017, *arXiv:1703.10400*
- Plavchan, P., Bilinski, C., & Currie, T. 2014, *PASP*, 126, 34
- Pollack, J. B., Hubickyj, O., Bodenheimer, P., et al. 1996, *Icarus*, 124, 62
- Ren, A., Fu, J., De Cat, P., et al. 2016, *ApJS*, 225, 28
- Sanchis-Ojeda, R., Rappaport, S., Winn, J. N., et al. 2014, *ApJ*, 787, 47
- Santerne, A., Moutou, C., Tsantaki, M., et al. 2016, *A&A*, 587, A64
- Santos, N. C., Israelian, G., & Mayor, M. 2004, *A&A*, 415, 1153
- Steffen, J. H., Ragozzine, D., Fabrycky, D. C., et al. 2012, *PNAS*, 109, 7982
- Su, D.-Q., & Cui, X.-Q. 2004, *ChJA&A*, 4, 1
- Twicken, J. D., Jenkins, J. M., Seader, S. E., et al. 2016, *AJ*, 152, 158
- Wang, S.-G., Su, D.-Q., Chu, Y.-Q., Cui, X., & Wang, Y.-N. 1996, *ApOpt*, 35, 5155
- Wang, J., & Fischer, D. A. 2015, *AJ*, 149, 14
- Wang, L., Wang, W., Wu, Y., et al. 2016, *AJ*, 152, 6
- Wang, W., Wang, L., Li, X. et al. Submitted
- Winn, J. N., & Fabrycky, D. C. 2015, *ARA&A*, 53, 409
- Xiang, M. S., Liu, X. W., Yuan, H. B., et al. 2015, *MNRAS*, 448, 822

Xie, J.-W., Dong, S., Zhu, Z., et al. 2016, PNAS, 113, 11431

Zhao, G., Zhao, Y.-H., Chu, Y.-Q., Jing, Y.-P., & Deng,
L.-C. 2012, RAA, 12, 723

Zhu, W., Wang, J., & Huang, C. 2016, ApJ, 832, 196